1991

A Mathematical Model of the Self-Discharge of a Ni-H2 Battery

Z. Mao
Texas A & M University - College Station

Ralph E. White
University of South Carolina - Columbia, white@cec.sc.edu

Publication Info

Journal of the Electrochemical Society, 1991, pages 3354-3361.

DOI: 10.1149/1.2085414
http://dx.doi.org/10.1149/1.2085414

anodic and cathodic currents were to be used as a model to define the rest potential, this occurrence would be consistent with a stabilized anodic curve and a cathodic curve that has been displaced downward to lower current values, as might be occasioned by the onset of porous film growth.

Summary

Anodic films of α-Al_2O_3 could be formed on only a fraction of aluminided Ni-200 specimens by constant current anodizing in molten sodium carbonate, the remaining specimens developing low-resistance NiO nodules which effectively shunted the anodizing current. Impedance spectra for the films for periods of immersion in sodium carbonate at 1000°C up to 25 h displayed both high-frequency and low-frequency arcs. The high-frequency behavior appears to represent the anodic oxide film, consistent with a film thickness in the 0.1-1 μm range that increases with time. At long immersion times impedance behavior resembles the nickel/sodium carbonate electrode, characterized by a Randles-like circuit containing an extra Warburg element and attributed to porous oxide growth. These measurements suggest that the initial anodizing process forms a barrier aluminum oxide film which grows by a thermally activated process on continued immersion in the carbonate. After approximately 45 h of immersion, the behavior changes and is consistent with the development of substantial porosity and continued film growth.

Manuscript submitted Jan. 30, 1991; revised manuscript received April 26, 1991.

REFERENCES

1. Chien-Tung Liu and Owen F. Devereux, *This Journal*, **138,** 386 (1991).
2. J. E. Lewis and R. C. Plumb, *ibid.*, **105,** 496 (1958).
3. J. A. Davies, J. P. S. Pringle, R. L. Graham, and F. Brown, *ibid.*, **109,** 999 (1962).
4. C. Y. Chao, L. F. Lin, and D. D. MacDonald, *ibid.*, **128,** 1187 (1981).
5. T. P. Hoar and N. F. Mott, *J. Phys. Chem. Solids*, **9,** 97 (1959).
6. D. A. Vermilyea, *This Journal*, **110,** 345 (1963).
7. M. A. Heine and M. J. Pryor, *ibid.*, **110,** 1205 (1963).
8. A. J. Brock and G. C. Wood, *Electrochim. Acta*, **12,** 395 (1967).
9. J. A. Davies and B. Domeij, *This Journal*, **110,** 849 (1963).
10. J. A. Davies, B. Domeij, J. P. S. Pringle, and F. Brown, *ibid.*, **112,** 675 (1965).
11. W. Ch. van Geel, *Physica*, **17,** 761 (1951).
12. W. Ch. van Geel, *Halbleiterprobleme*, **1,** 291 (1955).
13. R. L. Taylor and H. E. Haring, *This Journal*, **103,** 611 (1956).
14. Y. Sasaki, *J. Chem. Phys. Solids*, **13,** 177 (1960).
15. M. A. Heine and M. J. Pryor, *This Journal*, **110,** 1205 (1963).
16. C. J. Dell'oca and P. J. Fleming, *ibid.*, **123,** 1478 (1976).
17. S. Tajima, M. Soda, T. Mori, and N. Baba, *Electrochim. Acta*, **1,** 205 (1959).
18. S. Tajima, Y. Tanabe, M. Shimura, and T. Mori, *ibid.*, **6,** 127 (1962).
19. K. Y. Kim and O. F. Devereux, *Corros. Sci.*, **22,** 21 (1982).
20. K. Y. Kim and O. F. Devereux, *This Journal*, **125,** 1976 (1978).
21. H. M. Hindam and W. W. Smeltzer, *ibid.*, **127,** 1622 (1980).
22. C. E. Baumgartner, *ibid.*, **131,** 1850 (1984).
23. M. L. Orfield and D. A. Shores, *ibid.*, **135,** 1662 (1988).
24. M. L. Orfield and D. A. Shores, *ibid.*, **136,** 2862 (1989).
25. O. F. Devereux, K. Y. Kim, and K. S. Yeum, *Corros. Sci.*, **23,** 205 (1983).
26. R. D. Armstrong, M. F. Bell, and A. A. Metcalf, *J. Electroanal. Chem.*, **77,** 287 (1977).
27. W. D. Kingery, H. K. Bowen, and D. R. Uhlmann, "Introduction to Ceramics," p. 936, John Wiley & Sons, New York (1976).
28. R. J. Brook, J. Yee, and F. A. Kroeger, *J. Am. Ceram. Soc.*, **54,** 444 (1971).
29. M. G. S. R. Thomas, P. G. Bruce, and J. B. Goodenough, *This Journal*, **132,** 1521 (1985).
30. B. D. Cahan and C. T. Chen, *ibid.*, **129,** 474 (1982).

A Mathematical Model of the Self-Discharge of a Ni-H_2 Battery

Z. Mao* and R. E. White*

Center for Electrochemical Engineering, Department of Chemical Engineering, Texas A&M University, College Station, Texas 77843

ABSTRACT

A simple mathematical model is presented and used to characterize the self-discharge of a nickel oxyhydroxide (NiOOH) electrode in a hydrogen environment. This model includes diffusion of dissolved hydrogen in an electrolyte film which covers a flooded electrode, electrochemical oxidation of hydrogen, reduction of nickel oxyhydroxide, and changes of surface area and of porosity of the electrode during the self-discharge process. Although the self-discharge process is complicated, the predictions of the model are consistent with experimental results reported in the literature, which include linear relationships between the logarithm of hydrogen pressure and time and between the logarithm of the capacity remaining and time. The model predictions indicate that hydrogen oxidation takes place predominantly near the front side of the electrode, but the reduction of nickel oxyhydroxide to nickel hydroxide takes place uniformly throughout the electrode.

It is a commonly known that the self-discharge rate of a Ni-H_2 battery is many times higher than that of other batteries which use a NiOOH/$Ni(OH)_2$ electrode as the positive electrode, such as Ni-Cd, Ni-Fe, Ni-Zn, etc. This high self-discharge has imposed limits on applications of this battery, a problem which needs to be overcome. Previous investigations (1-5) into this area have contributed significantly to understanding of the self-discharge process, but discrepancies in interpretation of the phenomena exist from different experiments. Markin and Dell (3) reported that the diffusion of dissolved hydrogen has a significant effect on the self-discharge rate. They demonstrated that the self-discharge rate was substantially decreased when the nickel electrode was fully immersed in the electrolyte. The microcalorimetric measurements by Mao *et al.* (6) also showed such an effect of the electrolyte. However, Holleck (1) suggested that some kind of an interface reaction is the controlling step, because his theoretical calculation indicated that the self-discharge rate under diffusion control would be two orders of magnitude higher than that experimentally measured. Holleck's view on the self-discharge process was shared by many researchers in the Ni-H_2 battery community. That is, the self-discharge is a kinetically controlled process. However, the mechanism of hydrogen oxidation is far from being well understood. There are few investigations reported on this subject. Tsenter and Sluzhevskii (5) presented a set of kinetic equations to correlate self-discharge with the hydrogen pressure and the amount

* Electrochemical Society Active Member.

of undischarged NiOOH in the battery, with little attention being paid to the mechanism. By measuring the heat generation rate of β-NiOOH powder as well as a mixture of β-NiOOH and pure nickel powders in a hydrogen environment, Kim *et al.* (4) concluded that the mechanism of hydrogen oxidation is direct chemical reaction between hydrogen and nickel oxide material. More work is needed to characterize the self-discharge of a nickel electrode in hydrogen environment and to determine the mechanism. In this work, a simple mathematical model is presented to simulate the self-discharge process. The objective of this work is to gain a better understanding of the process so that an effective means can be taken to reduce the self-discharge rate.

Since the self-discharge always results in a corresponding drop of the hydrogen pressure in the cell, the overall reaction may be written as

$$H_2 + 2NiOOH \rightarrow 2Ni(OH)_2 \quad [1]$$

This reaction involves the transfer of two moles of electrons from H_2 to two moles of Ni^{3+}. It is possible that this reaction occurs via two electrochemical reactions as follows

$$H_2 + 2\,OH^- - 2e^- \rightarrow 2H_2O \quad [2]$$

$$2NiOOH + 2H_2O + 2e^- \rightarrow 2Ni(OH)_2 + 2\,OH^- \quad [3]$$

According to reaction [3], the reduction of nickel oxyhydroxide will occur regardless of the presence of hydrogen if the electrode potential is below the equilibrium potential of $NiOOH/Ni(OH)_2$. According to reaction [2], the oxidation of hydrogen does not depend on the availability of NiOOH if the electrode potential is high enough for hydrogen oxidation.

If the self-discharge process is due to a chemical reaction between hydrogen and NiOOH as shown in reaction [1], the local reaction rate in the nickel electrode would depend on the local hydrogen concentration and the local amount of NiOOH. The electrode potential would not affect the reaction rate, even though the potential of the electrode would change with the ratio of the amount of NiOOH to $Ni(OH)_2$ in the electrode. This chemical mechanism would be limited only to direct reaction between hydrogen and nickel oxyhydroxide; consequently, the local hydrogen oxidation rate would be exactly equal to the local reduction rate of nickel oxyhydroxide. If the self-discharge occurs electrochemically as shown by reactions [2] and [3], the local reaction rates of reactions [2] and [3] would depend on the local dissolved hydrogen concentration, the state of charge of the nickel electrode, and the electrode potential. The measured potential of the nickel oxyhydroxide electrode would be a mixed potential balanced by the polarizations of reactions [2] and [3] under the constraint of zero total current, depending on state of charge, self-discharge rate, and the reversibility of reaction [2] and [3]. In this work, the electrochemical mechanism is assumed to apply.

Mathematical Model

In the model presented here, the self-discharge process consists of the following steps (see Fig. 1). Hydrogen gas dissolves into the electrolyte and diffuses to the nickel electrode, where it is oxidized to form H_2O with OH^-. The nickel electrode is flooded and covered by a layer of electrolyte. Since the electrolyte is highly concentrated with potassium hydroxide (about 26-31 weight percent KOH), the solubility of hydrogen gas is small (about 10^{-4} M/atm). On the other hand, the self-discharge rate is also known to be small, which should not cause an appreciable change in KOH concentration. Therefore, the transport of dissolved hydrogen can be considered to be simple diffusion according to Fick's law

$$\frac{\partial \epsilon_s C_{H_2}}{\partial t} = \frac{\partial}{\partial x} D_{H_2} \epsilon_s^{\tau} \frac{\partial C_{H_2}}{\partial x} \quad [4]$$

where ϵ_s is the porosity of this electrolyte region which could represent the separator of the battery, and D_{H_2} is the diffusion coefficient of dissolved hydrogen in the electrolyte. This dissolved hydrogen is consumed by reaction [2] within the electrode. By measuring the short-circuit currents between the $NiOOH/Ni(OH)_2$ electrode and various other electrodes in hydrogen and argon environments, respectively, Lim concluded that the hydrogen oxidation occurs predominantly on the $NiOOH/Ni(OH)_2$ material (7). Mao and White (8) measured hydrogen oxidation currents at a $NiOOH/Ni(OH)_2$ electrode and a bare Ni sinter electrode at constant potentials, and found that the hydrogen oxidation current on a bare nickel electrode is much smaller than that on the $NiOOH/Ni(OH)_2$ electrode. Therefore, it seems reasonable to assume that the hydrogen oxidation process occurs in the nickel electrode on the $NiOOH/Ni(OH)_2$. A mass balance for the dissolved hydrogen in the electrode is given by

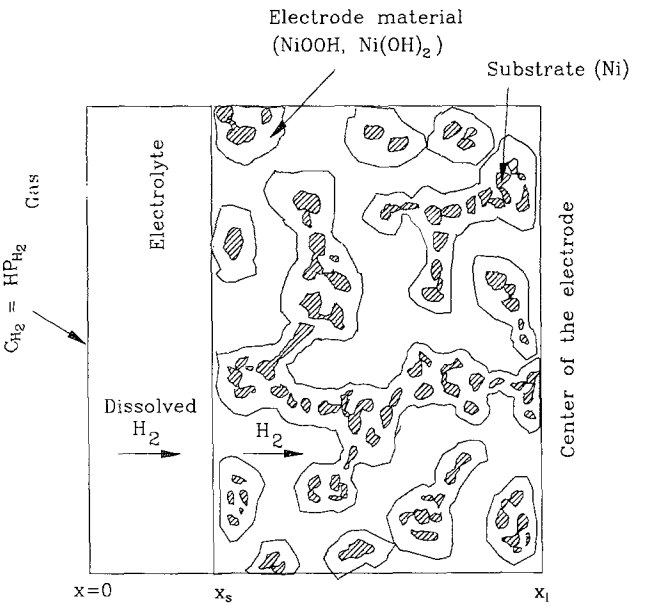

Fig. 1. Schematic of the hydrogen diffusion path and reaction zones.

$$\frac{\partial \epsilon C_{H_2}}{\partial t} = \frac{\partial}{\partial x} D_{H_2} \epsilon^{\tau} \frac{\partial C_{H_2}}{\partial x} - \frac{i_1}{2F} \quad [5]$$

where i_1 is the transfer current per unit volume of the electrode due to reaction [2], and can be expressed by

$$i_1 = i_{o1} a_1 \left(\frac{C_{H_2}}{C_{H_2,\,ref}} \right)^p \exp\left[\frac{\alpha_1 F}{RT} (E - E_{1,0}) \right] \quad [6]$$

where i_{o1} is the exchange current density for reaction [2], and $E_{2,o}$ is the equilibrium potential of reaction [2] at a reference condition (*e.g.*, at the initial hydrogen pressure). Since the electrode potential deviates far from the hydrogen equilibrium potential, the cathodic part of reaction [2] has been neglected.

Because nickel oxyhydroxide is continuously converted into less dense nickel hydroxide, the electrode becomes less porous, and consequently, the path for hydrogen diffusion in the electrode becomes narrower. The rate of change in the local porosity of the electrode can be calculated from the change in the material densities and the local self-discharge rate

$$\frac{\partial \epsilon}{\partial t} = \frac{i_2}{F} \left(\frac{M_{Ni(OH)_2}}{\rho_{Ni(OH)_2}} - \frac{M_{NiOOH}}{\rho_{NiOOH}} \right) \quad [7]$$

where $M_{Ni(OH)_2}$, M_{NiOOH}, $\rho_{Ni(OH)_2}$, and ρ_{NiOOH} are the molecular weights and the densities of nickel hydroxide and nickel oxyhydroxide, respectively. The symbol i_2 is the local transfer current per unit volume of the electrode due to reaction [3], and can be expressed by a modified Butler-Volmer equation (9)

$$i_2 = i_{o2} a_{max} x_{NiOOH}^{\beta_a} x_{Ni(OH)_2}^{1-\beta_a} \left\{ \exp\left[\frac{\beta_a F}{RT}(E - E_{2,e})\right] - \exp\left[-\frac{\beta_c F}{RT}(E - E_{2,e})\right] \right\} \quad [8]$$

where a_{max} is the nickel oxyhydroxide specific surface area when the electrode is fully charged, and $E_{2,e}$ is the equilibrium potential for reaction [3]. The mixing reaction between NiOOH and $Ni(OH)_2$ via proton diffusion is probably much faster than the self-discharge; consequently, the solid $NiOOH/Ni(OH)_2$ in the electrode is treated here as a homogeneous solid solution. That is, the equilibrium electrode potential for reaction [3] is given by the Nernst equation (10, 11)

$$E_{2,e} = E_{2,o} + \frac{RT}{F} \ln \frac{x_{NiOOH}}{x_{Ni(OH)_2}} = E_{2,o} + \frac{RT}{F} \ln \frac{(Q_{max} - Q)}{Q} \quad [9]$$

where x_{NiOOH} and $x_{Ni(OH)_2}$ represent the mole fractions of NiOOH and $Ni(OH)_2$, respectively, in the solid solution of the nickel electrode; $E_{2,o} = E_2^o - (RT/F) \ln [OH^-]$ with $[OH^-]$ assumed to be constant during the self-discharge (8 M here); Q represents the discharged capacity per unit volume of the elctrode; and Q_{max} is the total capacity per unit volume. To maintain a charge balance, the rate of a change in the local discharged capacity must be equal to the local transfer current due to reaction [3]

$$\frac{\partial Q}{\partial t} = -i_2 \quad [10]$$

When the local transfer currents, i_1 and i_2, differ in magnitude from each other, there must be a current flow in the solid phase along the electrode. Ohm's law governs such a current flow

$$\sigma \frac{dE}{dx} = -I \quad [11]$$

The rate of a change of the current density I with position must be equal to the sum of the local transfer currents, which yields

$$-\sigma \frac{d^2E}{dx^2} = i_1 + i_2 \quad [12]$$

Boundary conditions.—Hydrogen gas is assumed to be in equilibrium with dissolved hydrogen at the interface between the electrolyte and the gas phase ($x = 0$). The dissolved hydrogen diffuses into the bulk electrolyte and into the nickel electrode. The dissolution rate from the gas is equal to the diffusion rate in the electrolyte at the interface. **Under these conditions, the concentration of dissolved hydrogen satisfies the following equation at this boundary ($x = 0$, see Appendix for the derivation)**

$$-\left[(1 + ex)\frac{LQ_{max}}{2FP_{H_2}^o H}\right] \left.\frac{\partial C_{H_2}}{\partial t}\right|_{x=0} = -D_{H_2}\epsilon_s^\tau \frac{\partial C_{H_2}}{\partial x} \quad [13]$$

where L is the thickness of the electrode, $P_{H_2}^o$ is the initial hydrogen pressure, H represents Henry's constant, and ex is the fraction of excess hydrogen in the cell.

At the interface between the electrolyte and the electrode ($x = x_s$), the flux of dissolved hydrogen must be continuous. That is, the flux evaluated from the electrolyte side should be equal to that from the electrode side

$$D_{H_2}\epsilon_s^\tau \left.\frac{\partial C_{H_2}}{\partial x}\right|_{x_s^-} = D_{H_2}\epsilon^\tau \left.\frac{\partial C_{H_2}}{\partial x}\right|_{x_s^+} \quad [14]$$

Since electrical current in the electrode solid phase does not flow into the electrolyte layer near the electrode ($0 \le x \le x_s$), the derivative of the electrode potential must be zero at this interface

$$\sigma \left.\frac{\partial E}{\partial x}\right|_{x_s^+} = 0 \quad [15]$$

It is assumed here that the electrode plates are placed symmetrically in a Ni-H_2 battery, and that the boundary at $x = x_l$ is the center of the electrode. Therefore, both the flux of dissolved hydrogen and the current are equal to zero at the center of the electrode due to symmetry

$$D_{H_2}\epsilon^\tau \left.\frac{\partial C_{H_2}}{\partial x}\right|_{x_l^-} = 0 \quad [16]$$

$$\sigma \left.\frac{\partial E}{\partial x}\right|_{x_l^-} = 0 \quad [17]$$

Initial conditions.—The initial electrode potential is normally known, equal to a given value, and the initial state of charge is also known. The initial porosity of the electrode can be estimated based on a given loading of the active material and the porosity of the sinter nickel substrate. The initial concentration of dissolved hydrogen is not known except at the interface between the electrolyte and the gas, but it can be obtained by solving Eq. [4] and [5] at the given potential and the porosity at steady state. The values of the initial parameters and the fixed input parameters for the simulations in this study are given in Table I.

Solutions.—Equations [4], [5], [7], [10], and [12], together with [6], [8], and [9], are the governing equations for the electrode potential (E), the local discharged capacity (Q), the concentration of dissolved hydrogen (C_{H_2}), and the local porosity of the electrode (ϵ). Once the solutions of

Table I. Fixed parameters.

Symbol	Parameter	Reference
a_{max}	2.0×10^3 cm^2/cm^3	a
a_1	10^3 cm^2/cm^3	a
C_{KOH}	8M	
$C_{H_2,ref}$	2.75×10^{-6} mol/cm^3	b
D_{H_2}	1.53×10^{-5} cm^2/s	c
$E_{1,o}$	$-0.938 - \frac{RT}{F} \ln([OH^-]P_{H_2}^o)$ *vs.* Hg/HgO/1M KOH V	19
$E_{2,o}$	$0.42 - \frac{RT}{F} \ln [OH^-]$ *vs.* Hg/HgO/1M KOH V	19,d
ex	0.15	
H	$6.867 \times 10^{-7}/10^{0.137 C_{KOH}}$ mol/cm^3-atm	17
i_{o2}	10^{-4} A/cm^2	a
p	1.0	
Q_{max}	1300 C/cm^3	e
T	298.15 K	
x_s	0.01 cm	
x_l	0.05 cm	
α_1	$= \beta_a = \beta_c = 0.5$	a
ϵ^o	0.52	e
ϵ_s	1.0	
$\rho_{Ni(OH)_2}$	3.3 g/cm^3	18
ρ_{NiOOH}	3.8 g/cm^3	18
σ	10^4 S/cm	f
τ	1.5	15
	Initial parameters	
ϵ^o	$= 0.52$	
E^o	$= E_{3,o} + \frac{RT}{F} \ln \frac{Q_{max} - Q^o}{Q^o}$ V	
$P_{H_2}^o$	= 50 atm	
Q^o	$= 0.1\% Q_{max}$	

a: Arbitrarily chosen.
b: Calculated using $PO_{H_2}^o$ and Eq. [A-2].
c: Calculated using the theoretical equation in Ref. (16).
d: Based on $x_{NiOOH} = x_{Ni(OH)_2} = 0.5$
e: Calculated based on a capacity of 28.8 mAh/cm^2 for an electrode of thickness 0.08 cm. The porosity of the nickel sinter substrate was assumed to be 90%.
f: The conductivity of nickel metal is about 10^6 S/cm; the conductivity of the porous substrate was assumed to decrease proportionally to the porosity.

these equations subjected to the specific boundary and initial conditions are obtained, other variables such as the capacity remaining (C. R.), self-discharge rate (R_s), and hydrogen pressure (P_{H_2}) in the battery can be calculated using the following equations

$$P_{H_2} = C_{H_2}(0, t)/H \quad [18]$$

$$C.R. = \frac{Q_{max} - \frac{1}{x_l - x_s}\int_{x_s}^{x_l} Q dx}{Q_{max}} \times 100 \quad [19]$$

$$R_s = -\int_{x_s}^{x_l} i_2 dx = \int_{x_s}^{x_l} i_1 dx \quad [20]$$

After some preliminary computations, it was found that the concentration profile of dissolved hydrogen in the electrolyte layer is essentially linear. To simplify the computation and save computer time, Eq. [4] can be dropped by using a linear relation for C_{H_2} in the electrolyte layer and modifying the boundary condition at $x = x_s$ (see Appendix A)

$$-D_{H_2}\epsilon^{\tau}\frac{1}{x_s + \delta_t b_f}[C_{H_2}(x_s, t) - C_{H_2}(0, t - \delta_t)] = -D_{H_2}\epsilon^{\tau}\frac{\partial C_{H_2}}{\partial x}\bigg|_{x_s^+} \quad [21]$$

The governing equations and those for the boundary conditions were written in finite difference form using central and implicit backward differences in the spatial and time coordinates, respectively, and solved using the algorithm developed by Newman (12).

Model Predictions and Discussion

Predicted electrode potentials as a function of time are presented in Fig. 2 for different values of the exchange current density for hydrogen oxidation. As expected, the electrode potential changes rapidly in an early stage of the self-discharge, decreases slowly for a certain period, and finally, drops sharply when the electrode has lost almost all its capacity. The value of the exchange current density for hydrogen oxidation has a significant effect on the predicted electrode potential. For example, by increasing the exchange current density by one order of magnitude, the time for the loss of total capacity is reduced by about 200 h, and the electrode potential is lowered significantly. In an actual battery, hydrogen oxidation is a slow process which may consist of many steps and the exchange current density may be close to that for the slowest case in Fig. 2. A typical value of the self-discharge rate for a Ni-H_2 battery was reported to be about 10% of its capacity per day (4), which is equivalent to 0.1 mA/cm^2 for an electrode with a capacity of 24 mAh/cm^2. Assuming that the electrode thickness is 0.08 cm and the concentration of dissolved hydrogen is the same in the electrode as that at the interface

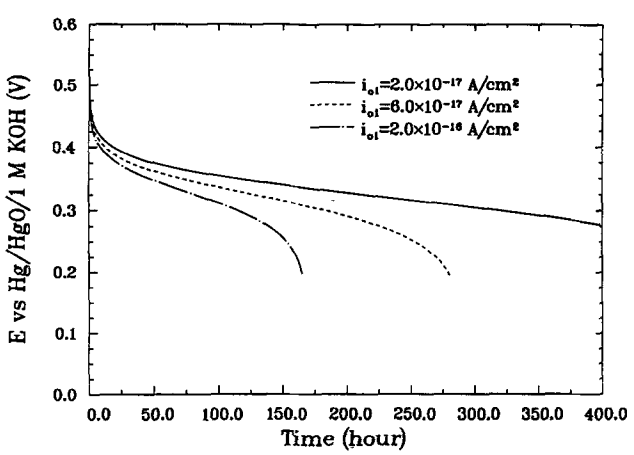

Fig. 2. Predicted electrode potentials as a function of time.

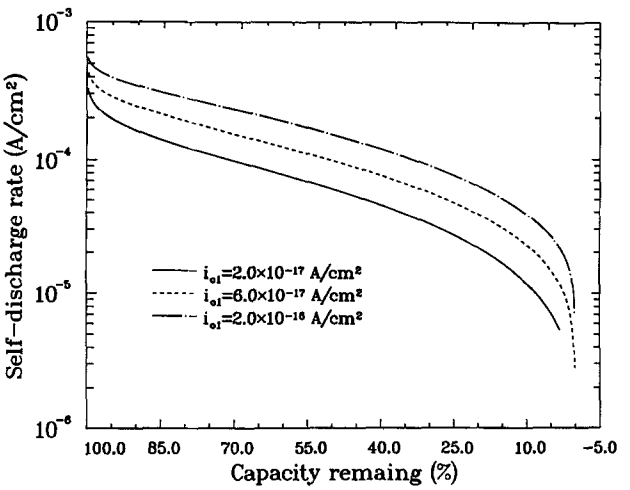

Fig. 3. Predicted dependence of the self-discharge rate on capacity remaining.

between the electrolyte and the gas phase, the exchange current density is estimated to be 2.17 × 10^{-18} A/cm^2 by using the parameters in Table I and solving Eq. [22] for i_{o1} at an electrode potential of 0.4V

$$I = Li_1 \quad [22]$$

where I represents the self-discharge rate in A/cm^2, L is the thickness of the electrode, and i_1 is the transfer current of hydrogen oxidation as expressed in Eq. [6]. It appears that the self-discharge reaction is kinetically controlled solely by the hydrogen oxidation. But, it still needs to be clarified whether the transport property of dissolved hydrogen has any effect on the self-discharge rate.

Figure 3 shows the predicted self-discharge rate as a function of the capacity remaining. Even though the relationship between the transfer current for the reduction of nickel oxyhydroxide and the capacity remaining is complicated in the mathematical model, the predicted self-discharge rate varies apparently linearly with the capacity remaining for certain portions of the curves, giving a first-order reaction with respect to the capacity remaining, a typical behavior of the self-discharge process as reported in literature (5, 14). The predicted hydrogen pressures as a function of time for various excess amounts of hydrogen are presented in Fig. 4(a)-(c), which are plotted in the same way as those previously reported for experimental results (1, 13). Visual inspection of Fig. 4(a) reveals that the logarithm of hydrogen pressure does not depend linearly on time. However, when the residual pressure (see List of Symbols for its definition) is subtracted from the total pressure, a plot of the logarithm of the hydrogen pressure difference *vs.* time shows a straight line for a certain period of time [see Fig. 4(b)]. Therefore, the linearity in the relationship between the logarithm of hydrogen pressure and time depends on the residual pressure. The self-discharge behavior is often characterized by the feature that the hydrogen pressure decreases linearly with the square root of time for approximately the first 50 h (13). Figure 4(c) shows such a linear behavior, except for late stages of the self-discharge and for the first few hours. The initial deviation from the linear behavior was observed by Lim (7). Figure 4(b) indicates that the more excess hydrogen is present, the faster the hydrogen pressure drops. This is because the self-discharge rate is higher when a large amount of hydrogen is present.

The logarithm of the predicted capacity remaining also has an approximately linear relationship with time, as shown in Fig. 5, which is qualitatively consistent with the experimental results reported by Stockel (14). However, it should be noted that this behavior of the self-discharge does not agree with the linear relationship between the logarithm of absolute hydrogen pressure and time reported by Holleck (1). According to the linear relation in Fig. 5, the self-discharge rate can be expressed simply by

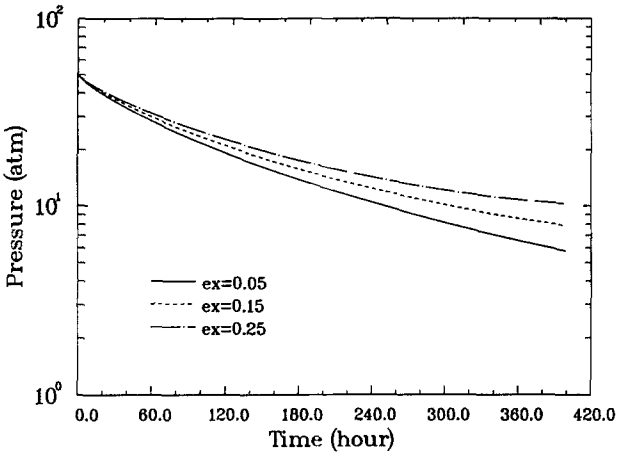

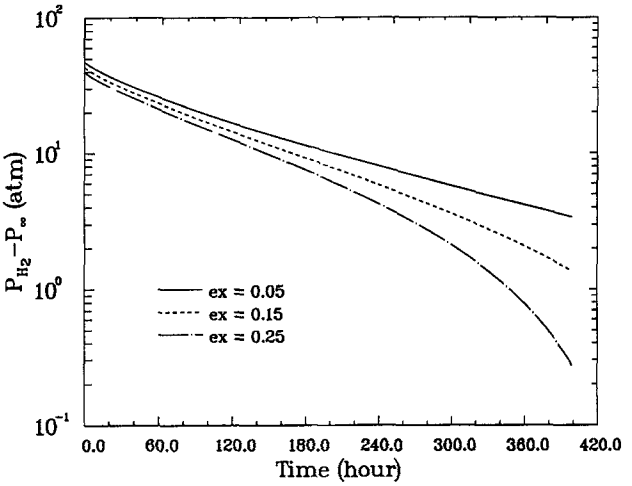

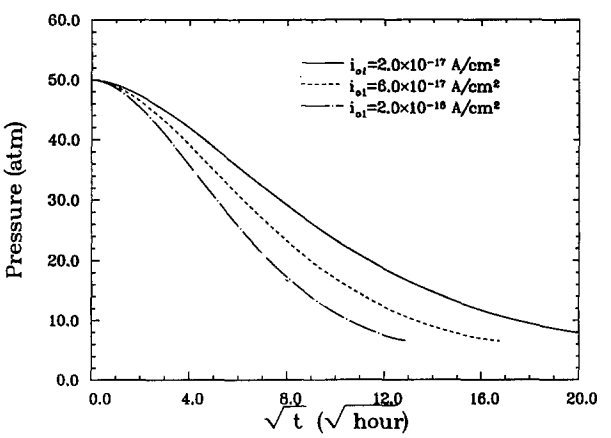

Fig. 4. (a) The logarithm of predicted hydrogen pressure *vs.* time, $i_{o1} = 2.0 \times 10^{-17}$ A/cm^2; (b) the logarithm of predicted hydrogen pressure difference between the total pressure and the residual pressure *vs.* time, $i_{o1} = 2.0^{-17}$ A/cm^2; (c) predicted hydrogen pressure as a function of square root of time.

$$-\frac{\partial}{\partial t}(Q_{max} - Q) = k(Q_{max} - Q) \qquad [23]$$

where $Q_{max} - Q$ represents the undischarged capacity, and k is the slope of the curve. Assuming an ideal gas for hydrogen, the capacity remaining can be expressed in terms of the hydrogen pressure

$$Q_{max} - Q = A(P_{H_2} - P_\infty) \qquad [24]$$

where P_∞ is the residual pressure, and A is a proportional constant. Substitution of Eq. [24] into [23] yields

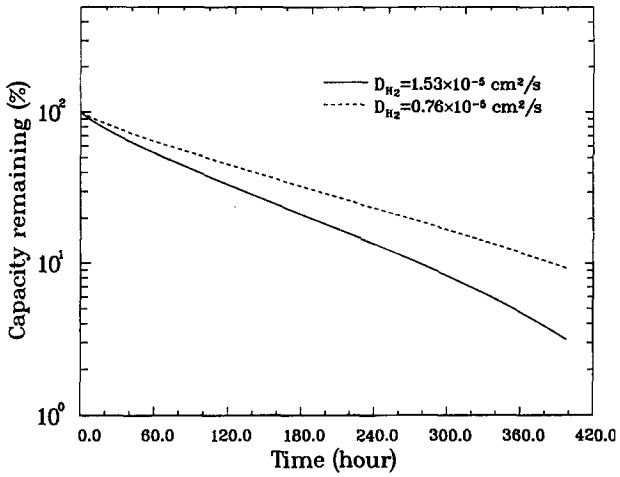

Fig. 5. The logarithm of predicted capacity remaining as a function of time for different diffusion coefficients of dissolved hydrogen.

$$-\frac{\partial P_{H_2}}{\partial t} = k(P_{H_2} - P_\infty) \qquad [25]$$

Obviously, the logarithm of absolute hydrogen pressure is not linearly proportional to time, but the logarithm of the pressure difference between the absolute value and the residual pressure has a linear behavior. Figure 5 also indicates that the transport property of dissolved hydrogen has a significant effect on the self-discharge rate. The capacity remaining decreases more slowly for the smaller diffusion coefficient.

Figure 6 presents the predicted self-discharge rate as a function of time for different thicknesses of the electrolyte layer on the electrode. As expected, the logarithm of the self-discharge rate decreases linearly with time. The thickness of the electrolyte layer slightly affects the self-discharge rate. The self-discharge rate decreases more rapidly for a thin electrolyte layer than a thick electrolyte layer, because the former enables dissolved hydrogen to diffuse quickly to the electrode, resulting in a higher self-discharge rate initially. However, when the self-discharge rate becomes small, the reaction becomes more kinetically controlled, and consequently, the self-discharge rate becomes smaller for the thin electrolyte layer than for a thick electrolyte layer, because in the latter there is more hydrogen present in the cell.

The self-discharge rate for a nickel electrode can be directly determined by measuring the heat generation rate of the electrode in a hydrogen environment. Mao *et al.* (6) did

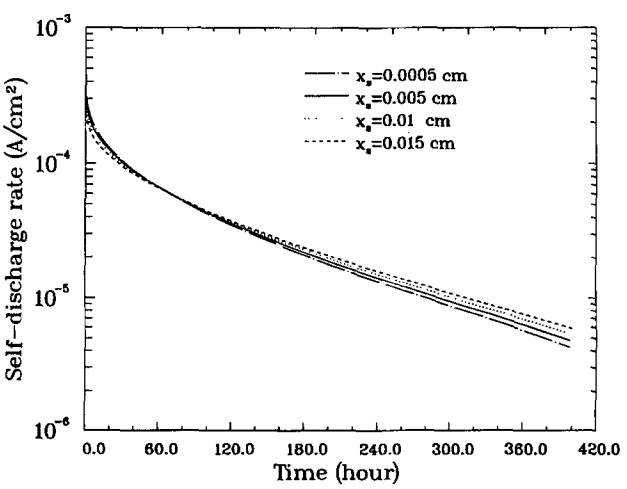

Fig. 6. Predicted self-discharge rates as a function of time for different thicknesses of the electrolyte layer on the electrode. $i_{o1} = 2.0 \times 10^{-17}$ A/cm^2.

such measurements with a microcalorimeter under constant hydrogen pressures, and found that the self-discharge rate can be fitted with a simple equation

$$R_s = a + b \exp(kt) \quad [26]$$

where a, b, and k are constant, and their values depend on experimental conditions such a hydrogen pressure and electrode immersion state in the electrolyte. To determine whether the model presented in this work can predict the self-discharge behavior as observed in the microcalorimetric experiments, the flux boundary condition (Eq. [13]) was changed to a fixed boundary condition. That is

$$C_{H_2}|_{x=0} = HP^{\circ}_{H_2} \quad [27]$$

The curves predicted from the model presented here and that given by Eq. [26] are presented in Fig. 7, where $a = 0.1435$ mA/cm^2-s, $b = 0.0939$ mA/cm^2-s, and $k = -0.2029$ h^{-1}. It can be seen that these two curves match well with each other. This means that the self-discharge rate as a function of time as measured by a microcalorimeter is of the same shape as that predicted by the model presented here.

It is often thought that the concentration gradient of dissolved hydrogen is minimal, and that the diffusion of dissolved hydrogen would least affect the self-discharge rate because the self-discharge rate is small. However, the predicted concentration profile for dissolved hydrogen reveals a profound gradient, as shown in Fig. 8(a). This result is directly attributed to a small solubility of hydrogen gas in the concentrated alkaline solution and a small diffusion coefficient of dissolved hydrogen. Under hydrogen diffusion control, the maximum diffusion rate across an electrolyte layer of 0.01 cm is estimated to be 0.182 mA/cm^2 at a hydrogen pressure of 50 atm. This value is higher by one order of magnitude less than that corresponding to 10% capacity loss per day. Therefore, the diffusion of dissolved hydrogen still controls partially the self-discharge rate, particularly at early stages of the self-discharge process. Although Fig. 8(a) also shows that the concentration profile becomes almost flat when the electrode looses nearly the entire capacity, the self-discharge rate is very small at this state of charge and does not represent the overall self-discharge rate. Contrary to the concentration profile of dissolved hydrogen, the porosity distribution is uniform throughout the electrode, as shown in Fig. 8(b). Since a uniform initial porosity was assumed, and the electrode is highly conductive, the driving force for the reduction of nickel oxyhydroxide remains constant along the electrode, resulting in a uniform transfer current for the reaction.

Figure 9 shows the distribution of the transfer current for hydrogen oxidation in the electrode. It can be seen that the oxidation of dissolved hydrogen takes place predominantly near the front side of the electrode, initially, and penetrates gradually into the electrode. The transfer current distribution becomes flat when the transfer current becomes small and the electrode has lost most of its capacity.

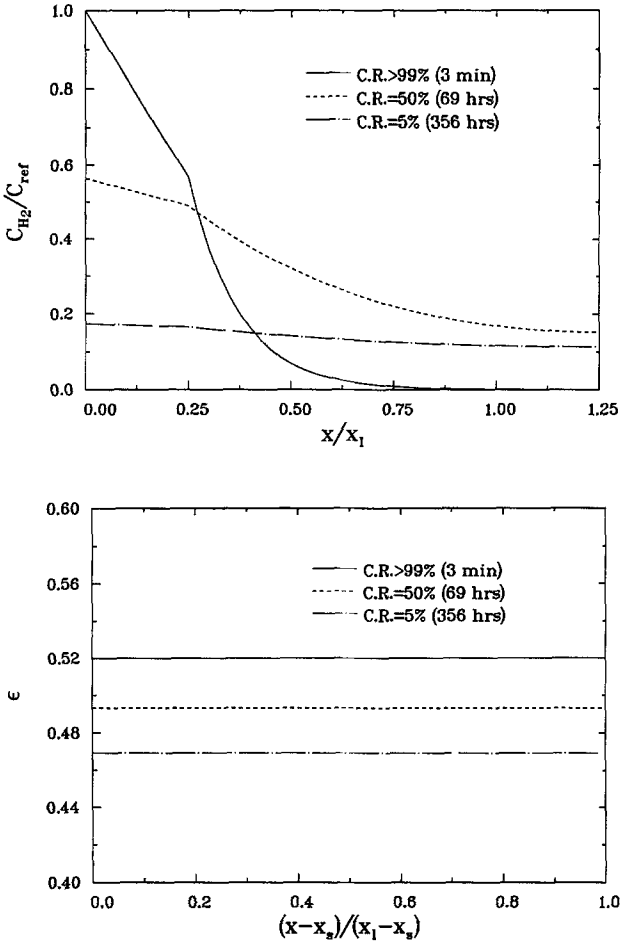

Fig. 8. (a) The concentration distribution of dissolved hydrogen; (b) the porosity distribution at different times. $i_{o1} = 2 \times 10^{-17}$ A/cm^2.

Conclusions

A simple mathematical model has been presented and used to predict the self-discharge behavior of a Ni-H_2 battery. The model predictions are consistent qualitatively with experimental results reported in the literature. These include linear relationships between time and the logarithm of the self-discharge rate, the logarithm of the capacity remaining, and the square root of hydrogen pressure. Since some parameters such as the thickness of the electrolyte layer (x_s) and the effective specific electrode sur-

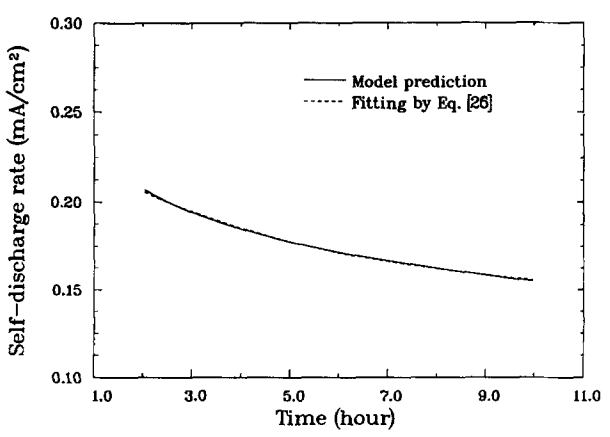

Fig. 7. Predicted self-discharge rate as a function of time under constant hydrogen pressure, $P_{H_2} = 50$ atm, $i_{o1} = 2.0 \times 10^{-17}$ A/cm^2.

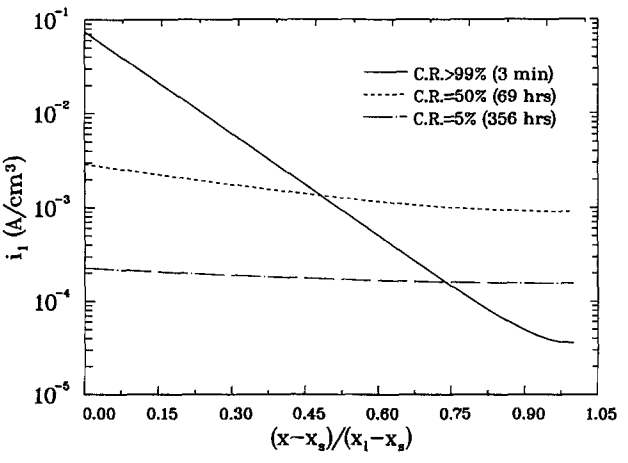

Fig. 9. The transfer current distribution for hydrogen oxidation at different states of charge. $i_{o1} = 2 \times 10^{-17}$ A/cm^2.

face area are difficult to determine, no attempt was made to fit the model predictions to any experimental data. Comparisons between the model predictions and experimental data are limited to qualitative agreement.

The concentration gradient of dissolved hydrogen in the electrolyte layer and electrode is large, particularly at an early stage of the self-discharge process, even though the self-discharge rate is small, because the hydrogen solubility and the diffusion coefficient of dissolved hydrogen are small. The thickness of an electrolyte layer on the electrode does not significantly affect the overall self-discharge rate. Any means which can reduce the diffusion of dissolved hydrogen can reduce the self-discharge rate, particularly for electrodes at high states of charge. The dependence of the logarithm of hydrogen pressure on time is apparently not linear, but the logarithm of hydrogen pressure minus a residual pressure shows a linear relation with time. Such behavior is consistent with other features of the self-discharge process, such as the relation between the capacity remaining and time.

Acknowledgments

The authors are grateful for the financial support of this work from the Hughes Aircraft Company and the NASA Center for Space Power at Texas A&M University.

Manuscript submitted March 25, 1991; revised manuscript received May 28, 1991.

Texas A&M University assisted in meeting the publication costs of this article.

APPENDIX

Derivation of the Boundary Conditions at x = 0 and x = x_s

Hydrogen gas dissolves into the electrolyte at the interface between the electrolyte and gas phase (at $x = 0$), and the consumption rate of hydrogen gas must be equal to the hydrogen diffusion rate at the interface multipled by the total area of the interface. Assuming that dissolved hydrogen is in equilibrium with hydrogen gas at this interface, and that the gas is ideal, the following equations are valid

$$-\frac{\partial n_{H_2}}{\partial t} = -SD_{H_2}\epsilon_s^{\tau}\left.\frac{\partial C_{H_2}}{\partial x}\right|_{x=0} \quad [A\text{-}1]$$

$$C_{H_2}(0, t) = HP_{H_2} \quad [A\text{-}2]$$

$$n_{H_2} = \frac{VP_{H_2}}{RT} \quad [A\text{-}3]$$

Substituting Eq. [A-3] and [A-2] into [A-1] to eliminate n_{H_2} yields the equation

$$-\frac{V}{S}\frac{1}{RTH}\frac{\partial C_{H_2}}{\partial t} = -D_{H_2}\epsilon_s^{\tau}\frac{\partial C_{H_2}}{\partial x} \quad [A\text{-}4]$$

Although the actual volume of hydrogen gas is unknown, the ratio of V to S can be eliminated from Eq. [A-4] using the initial material balance as follows

$$n_{H_2}^{o} = \frac{VP_{H_2}^{o}}{RT} = (1 + ex)S\frac{Q_{max}L}{2F} \quad [A\text{-}5]$$

$$\frac{V}{S} = (1 + ex)RT\frac{Q_{max}L}{2FP_{H_2}^{o}} \quad [A\text{-}6]$$

where ex represents the fraction of the excess amount of hydrogen present in the cell. Substitution of Eq. [A-6] into [A-4] yields the boundary condition at $x = 0$

$$-\left[(1 + ex)\frac{LQ_{max}}{2FP_{H_2}^{o}H}\right]\left.\frac{\partial C_{H_2}}{\partial t}\right|_{x=0} = -D_{H_2}\epsilon_s^{\tau}\frac{\partial C_{H_2}}{\partial x} \quad [A\text{-}7]$$

If the concentration profile is linear in the electrolyte region, and the derivative of the concentration with respect to time is expressed in backward difference form with a time step size of ∂_t, one obtains the following equations

$$\left.\frac{\partial C_{H_2}}{\partial x}\right|_{x=0} = \frac{C_{H_2}(x_s, t) - C_{H_2}(0, t)}{x_s} \quad [A\text{-}8]$$

$$\left.\frac{\partial C_{H_2}}{\partial t}\right|_{x=0} = \frac{C_{H_2}(0, t) - C_{H_2}(0, t - \delta_t)}{\delta_t} \quad [A\text{-}9]$$

Substitution of Eq. [A-8] and [A-9] into [A-7] gives

$$C_{H_2}(0, t) - C_{H_2}(0, t - \delta_t) = \frac{\partial_t b_f}{x_s}(C_{H_2}(x_s, t) - C_{H_2}(0, t)) \quad [A\text{-}10]$$

where

$$b_f = \frac{D_{H_2}\epsilon_s^{\tau}}{\left[(1 + ex)\frac{LQ_{max}}{2FP_{H_2}^{o}H}\right]} \quad [A\text{-}11]$$

Solving Eq. [A-10] for $C_{H_2}(0, t)$ gives

$$C_{H_2}(0, t) = \frac{C_{H_2}(x_s, t)\frac{\delta_t b_f}{x_s} + C_{H_2}(0, t - \delta_t)}{1 + \frac{\delta_t b_f}{x_s}} \quad [A\text{-}12]$$

At the boundary, $x = x_s$, Eq. [14] can be expressed as

$$D_{H_2}\epsilon_s^{\tau}\frac{C_{H_2}(x_s, t) - C_{H_2}(0, t)}{x_s} = D_{H_2}\epsilon^{\tau}\left.\frac{\partial C_{H_2}}{\partial x}\right|_{x_s^+} \quad [A\text{-}13]$$

Substituting of Eq. [A-12] into [A-13] yields the boundary condition at $x = x_s$

$$-D_{H_2}\epsilon^{\tau}\frac{1}{x_s + \delta_t b_f}[C(x_s, t) - C_{H_2}(0, t - \delta_t)] = -D_{H_2}\epsilon^{\tau}\left.\frac{\partial C_{H_2}}{\delta x}\right|_{x_s^+} \quad [A\text{-}14]$$

LIST OF SYMBOLS

a	constant, A/cm^2-s
a_{max}	maximum electrode surface area per unit volume of the nickel electrode for the nickel oxide reduction, cm^2/cm^3
a_1	electrode surface area per unit volume of the nickel electrode for the hydrogen oxidation, cm^2/cm^3
b	constant, A/cm^2-s
b_c	intercalation coefficient, V
b_c^*	intercalation coefficient, V/C
C_{H_2}	the concentration of dissolved hydrogen, mol/cm^3
$[OH^-]$	the concentration of hydroxide ions, mol/l
$C_{H_2,ref}$	reference concentration of dissolved hydrogen, mol/cm^2
D_{H_2}	diffusion coefficient of dissolved hydrogen, cm^2/s
ex	fraction of excess hydrogen
E	electrode potential (potential of the solid phase relative to the potential in the adjacent solution phase), V
E^o	initial electrode potential, V
$E_{1,o}$	equilibrium potential of hydrogen oxidation at the nickel electrode for a given electrolyte, V
$E_{2,e}$	the equilibrium nickel electrode potential at a given state of charge, V
$E_{2,o}$	the equilibrium nickel electrode potential at the standard condition, V
F	Faraday's constant, 96,487 C/equivalent
H	Henry's constant, mol/cm^3-atm
I	current density relative to the projected area of the electrode in the solid phase of the electrode, A/cm^2
i_{o1}	exchange current density for hydrogen oxidation evaluated at a reference hydrogen concentration, A/cm^2
i_{o2}	exchange current density for the nickel electrode reaction, A/cm^2
i_1	local transfer current per unit volume of the electrode for hydrogen oxidation, A/cm^3
i_2	local transfer current per unit volume of the electrode for the reduction of nickel oxyhydroxide, A/cm^3
k	constant, s^{-1} (Eq. [23]), h^{-1} (Eq. [26]).
L	thickness of nickel oxyhydroxide electrode
$M_{Ni(OH)_2}$	the molecular weight of $Ni(OH)_2$
M_{NiOOH}	the molecular weight of NiOOH
$n_{H_2}^o$	initial amount of hydrogen gas in the cell, mol
p	reaction order with respect to the concentration of dissolved hydrogen

P_{H_2} hydrogen pressure in the cell, atm
$P^o_{H_2}$ initial hydrogen pressure in the cell, atm
P_∞ the residual hydrogen pressure in the cell after the cell has been completely discharged, atm
Q discharge capacity per unit volume of the nickel electrode, C/cm^3
Q^o initial discharge capacity per unit volume of the nickel electrode, C/cm^3
Q_{max} total capacity per unit volume of the nickel electrode, C/cm^3
R universal gas constant, 8.314 J/mol-K
R_s self-discharge rate, A/cm^2
S total geometric electrode area in the cell, cm^2
V volume of hydrogen gas in the cell, cm^3
x_s the thickness of the electrolyte layer, cm
x_l $L/2 + x_s$, cm
x_{NiOOH} mole fraction of NiOOH in the solid solution of the nickel electrode
$x_{Ni(OH)_2}$ mole fraction of $Ni(OH)_2$ in the solid solution of the nickel electrode

Greek Letters

α_l transfer coefficient for hydrogen oxidation at the nickel electrode
β_a anodic transfer coefficient for the nickel oxyhydroxide reduction
β_c cathodic transfer coefficient for the nickel oxyhydroxide reduction
δ_t step size in the time coordinate, s
ϵ^o initial porosity of the nickel electrode
ϵ local porosity of the nickel electrode
ϵ_s porosity of the electrolyte layer
ξ exponential term to correct properly an change in the electrode surface area
$\rho_{Ni(OH)_2}$ density of nickel hydroxide, g/cm^3
ρ_{NiOOH} density of nickel oxyhydroxide (NiOOH), g/cm^3
σ conductivity of the nickel electrode, S/cm
τ exponential term to correct the effective hydrogen diffusion coefficient

REFERENCES

1. G. Holleck, Proceedings of 1977 Goddard Space Flight Center Battery Workshop, p. 525, NASA Conference Publication 2041 (1977).
2. C. Iwakura, Y. Kajiya, H. Yoneyama, T. Sakai, K. Oguro, and H. Ishikawa, *This Journal*, **136,** 1351 (1989).
3. T. L. Markin and R. M. Dell, *J. Electroanal. Chem.*, **118,** 217 (1981).
4. Y. Kim, A. Visintin, S. Srinivasan, and A. J. Appleby, in "Nickel Hydroxide Electrodes," (PV 90-4) D. A. Corrigan and A. H. Zimmerman, Editors, p. 368, The Electrochemical Society Softbound Proceedings Series, Pennington, NJ (1990).
5. B. I. Tsenter and A. I. Sluzhevskii, *Zh. Prikl. Khim*, **54,** 2250 (1981).
6. Z. Mao, S. Visintin, S. Srinivasan, and A. J. Appleby, *J. Appl. Electrochem.*, Submitted.
7. H. Lim, Unpublished data, Hughes Aircraft Company, Torrance, California.
8. Z. Mao and R. E. White, *This Journal*, To be submitted.
9. T. V. Nguyen, Ph.D. Dissertation, Texas A&M University, College Station, TX (1988).
10. R. Barnard, C. F. Randell, and F. L. Tye, *J. Appl. Electrochem.*, **10,** 127 (1980).
11. J. Bouet, F. Richard, and Ph. Blanchard, in "Nickel Hydroxide Electrodes," (PV 90-4) D. A. Corrigan and A. H. Zimmerman, Editors, p. 260, The Electrochemical Society Softbound Proceedings Series, Pennington, NJ (1990).
12. J. S. Newman, "Electrochemical Systems," Appendix C, Prentice-Hall, Inc., Englewood Cliffs, NJ (1973).
13. P. E. Ritterman and A. M. King, Proceedings of the 20th InterSociety Energy Conversion Engineering Conference, p. 1175 (Aug., 1985).
14. J. F. Stockel, *ibid.*, p. 1171.
15. W. G. Sunu, Ph.D. Dissertation, University of California, Los Angeles (1978).
16. "Chemical Engineering Handbook," 5th Ed., R. H. Perry and C. H. Chilton, Editors, p. 3-234, McGraw Hill, New York (1973).
17. R. Battio and E. Wilhelm, "IUPAC Solubility Data Series," Vol. 5/6, C. L. Young, Editor, p. 33, Pergamon Press, New York (1981).
18. A. H. Zimmerman and P. K. Effa, Abstract 28, p. 43, The Electrochemical Society Extended Abstracts, Vol. 85-2, Las Vegas, NV, Oct. 13-18, 1985.
19. S. G. Bratsch, *J. Phys. Chem. Ref. Data*, **18,** 1 (1989).

Reaction Mechanisms at the n-FeS_2/I Interface

An Electrolyte Electroreflectance Study

P. Salvador and D. Tafalla

Instituto de Catalisis y Petroleoquimica (CSIC), Serrano, 119, 28006-Madrid, Spain

H. Tributsch and H. Wetzel

Hahn-Meitner-Institut, D-1000 Berlin 39, Germany

ABSTRACT

Monocrystalline n-FeS_2 (pyrite) in contact with the I^-/I_n^- redox couple was studied by electrolyte electroreflectance (EER) and conventional electro- and photoelectrochemical techniques. The EER signal originating from the 3.13 eV S: p → Fe: e_g, direct transition in pyrite can be used to determine precisely its flatband potential (V_{FB}), even in the presence of a high concentration of bandgap surface states, which is typical for this semiconducting transition metal sulfide. We have also been able to show that dynamic V_{FB} measurements are possible under situations where capacitance studies are extremely complicated. Experimental evidence is given on strong interaction of I^- and I_n^--ions with the FeS_2 surface, via complex formation with Fe^{3+} lattice ions generated by hole capture during anodic polarization or illumination. Small V_{FB} shifts of about 50 mV toward negative potentials indicate that specific adsorption is stronger for I_n^- than for I^- species. Moreover, V_{FB} shifts of more than 1 V towards negative values can also be observed under cathodic polarization. This behavior is correlated to surface accumulation of electrons which accompanies FeS_2 electroreduction. A comprehensive model for surface photoreactions is proposed. This takes into account the catalytic role of the semiconductor surface in kinetics of charge transfer to the electrolyte. Both the very positive V_{FB} (high electronic affinity) and the high density of bandgap states, probably associated with Fe_2S_3 lattice impurities, seem to determine the photovoltage limitations which are inherent to the FeS_2/I^- system.

Transition metal chalcogenides with d-band character are known to be characterized by a high density of surface states (1). Accumulation of electric charge is found with each surface transition metal, which may lead to drastic shifts of the flatband potential. This property makes the application of conventional electrochemical techniques for flatband determination (Mott-Schottky plots) questionable and frequently impossible. Since the understanding